Applied Surface Science 499 (2020) 143859

Contents lists available at ScienceDirect

Applied Surface Science

journal homepage: www.elsevier.com/locate/apsusc

Full length article

Ab-initio approach to the stability and the structural, electronic and magnetic properties of the (001) $Znfe_2O_4$ surface terminations

K.L. Salcedo Rodríguez[a], J.J. Melo Quintero[a], H.H. Medina Chanduví[a], A.V. Gil Rebaza[a,b], R. Faccio[c], W.A. Adeagbo[d], W. Hergert[d], C.E. Rodríguez Torres[a], L.A. Errico[a,e,*]

[a] Instituto de Física La Plata (IFLP) y Departamento Física, Facultad de Ciencias Exactas, Universidad Nacional de La Plata (UNLP)-CCT La Plata CONICET, C.C. 67, CP 1900 La Plata, Argentina
[b] Grupo de Estudio de Materiales y Dispositivos Electrónicos (GEMyDE), Dpto. de Electrotecnia, Fac. de Ingeniería, UNLP, Argentina
[c] Centro NanoMat-DETEMA, Facultad de Química, Universidad de la República, Uruguay
[d] Institut of Physik, Martin-Luther-Universitaet Halle-Wittenberg, Von-Seckendorff-Platz 1, 06120 Halle, Germany
[e] Universidad Nacional del Noroeste de la Provincia de Buenos Aires (UNNOBA), Monteagudo 2772, Pergamino CP 2700, Buenos Aires, Argentina

ARTICLE INFO

Keywords:
Zn-ferrite
Surface termination
Electronic structure
Magnetic response
Ab initio

ABSTRACT

We present a Density Functional Theory (DFT) based study of the structural and magnetic properties of the (001) surface of the semiconducting oxide $ZnFe_2O_4$ (spinel structure). The calculations were performed using the DFT based ab initio plane wave and pseudopotential method as implemented in the Quantum Espresso code. The all electron Full-potential linearized-augmented-plane-wave method (FP-LAPW) was also employed to check the reproducibility of the plane wave method. In both calculations the DFT + U methodology was employed and different (001) surface terminations of $ZnFe_2O_4$ were studied. We find that the surface terminated in Zn is the stable one. For all the (001) surface terminations our calculations predict that the Zn-Fe cationic inversion (anti-sites), which are defects in bulk $ZnFe_2O_4$, becomes stable and an integral part of the surface. Also, a ferrimagnetic behavior is predicted for the case of anti-sites in the superficial layer. Our results for different properties of the surface of $ZnFe_2O_4$ are compared with those obtained in bulk samples and those reported in the literature.

1. Introduction

Due to their electronic, optical and magnetic properties, ferrites (XFe_2O_4 X: Zn, Co, Ni, Al, Mg, Ti, among others [1]) are very interesting materials both from a fundamental and application point of view. In the last decades, progress in synthesis process renews the interest in this kind of insulating oxides and improves their physical properties, expanding their applications to new areas [2–4]. Particularly, zinc ferrite ($ZnFe_2O_4$) is of interest not only in basic research due to its intriguing magnetic behavior [5–11] but also has great potential in technological applications [12–15].

$ZnFe_2O_4$ crystallize in the spinel-type structure in which the cations occupy tetrahedral and octahedral sites (A and B sites, respectively) [1]. In terms of the sites, the cation distribution can be described by the formula $(Zn_{1-\alpha}Fe_\alpha)[Zn_\alpha Fe_{2-\alpha}]O_4$ where round and square brackets denote A and B sites and α is the inversion parameter. For $\alpha = 0$ the Zn atoms occupy the A sites and the Fe atoms the B ones (normal $ZnFe_2O_4$). For $0 < \alpha < 1$ some percentage of the Zn atoms are located at the B sites instead of the A sites and corresponding concentration of Fe then occupies A sites (partially inverted structure). In the case of $\alpha = 1$, all the A sites are occupied by Fe atoms. $ZnFe_2O_4$ belongs to the class of normal ferrites, but, depending on the sample preparation method and on the thermal treatment, some degree of inversion could appear. In no-defective bulk $ZnFe_2O_4$ the absence of Fe atoms at A sites (populated by non-magnetic Zn atoms) results in weak antiferromagnetic exchange interactions between the Fe atoms via intermediate oxygen anions (Fe^B-O-Fe^B interactions, being Fe^B iron cations located at the B sites), making ZFO a strongly paramagnetic oxide with antiferromagnetic coupling only below about 10 K [16] and a quite complex ground state ([17,18] and Refs. therein). However, when particle size is reduced to the nano-scale some degree of inversion that may scale with the surface area of the samples is observed [19–21]. The presence of inversion gives rise to Fe^B-O-Fe^A and Fe^A-O-Fe^A couplings, enhancing the magnetic interactions and the ferrimagnetic behavior at high temperatures [20].

* Corresponding author at: Universidad Nacional del Noroeste de la Provincia de Buenos Aires (UNNOBA), Monteagudo 2772, Pergamino CP 2700, Buenos Aires, Argentina.
E-mail address: errico@fisica.unlp.edu.ar (L.A. Errico).

https://doi.org/10.1016/j.apsusc.2019.143859
Received 5 March 2019; Received in revised form 23 July 2019; Accepted 2 September 2019
Available online 03 September 2019

In this work, our aim is to understand, by means of ab initio calculations, the structure at the atomic scale (which has remained unsolved) and the stable termination of the (001) surface of $ZnFe_2O_4$. Additionally, it is relevant to know how the surface termination affects the structural and electronic properties of the near surface layers, the cation inversion degree and the magnetic response of the system.

2. Calculations details

The spinel structure, *Fd3m* (*Oh7*), of $ZnFe_2O_4$ is characterized by two parameters, the lattice constant a (8.43–8.46 Å, see Refs. [8,22–25]) and the oxygen position parameter u (0.258, Ref. [25]). The unit cell contains eight formula units (56 atoms). More details of the structure can be found in Reference [17]. Our aim here is to study the (001) surface of $ZnFe_2O_4$ and how the surface affects the formation of defects (cationic inversion and oxygen vacancies in the present case). Two types of (001) surface terminations can be obtained from a bulk truncation of $ZnFe_2O_4$: the fully Zn-terminated surface (Zn_2) or an O_4-Fe_4-O_4 termination that "exposes" O and Fe atoms. In order to study the effect of a reducing atmosphere, a O_4-Fe_4 termination was study. This termination was obtained by removing the four external oxygen atoms from the O_4-Fe_4-O_4 termination. These surface terminations are shown in Fig. 1. In order to study these (001) surface terminations ab initio calculations have been performed on the basis of Density Functional Theory (DFT) using two different methods of calculation, the Full-Potential Linearized Plane Waves method (FP-LAPW) [26–28] as implemented in Wien2k code [29] and the plane wave and pseudopotential method as implemented in Quantum-Espresso code (QE, Refs. [30] and [31]). The first method is recognized as one of the more accurate for the determination of the electronic structure of solids but is computationally expensive and time consuming when large systems or systems that present low symmetries or reduced dimensions (as in the case of surfaces). The plane wave and pseudo-potential methods is more flexible to study structural and electronic properties of complex systems. To be on the safe side, however, we need to verify first whether this fast and more approximative method correctly reproduces some key properties predicted by the more accurate FP-LAPW method.

In the case of the ab initio plane wave and pseudopotential calculations the exchange and correlation effects were treated within density-functional theory using Perdew-Burke-Ernzerhof (PBE) [32] parameterization of the generalized gradient approximation plus the Hubbard U term (GGA + U) in the self-interaction correction (SIC) scheme [33] with $U = 5$ eV [17] for the Fe-3*d* orbitals. The ionic cores were described using ultrasoft pseudo-potentials from the Standard Solid State Pseudopotentials library (SSSP, Ref. [34]), where the converged kinetic energy cutoff for the wavefunction and charge density were set to 70 Ry and 500 Ry, respectively. For the electronic integration, the irreducible Brillouin zone was described according to the Monkhorst-Pack scheme [35] using a $2 \times 2 \times 1$ k-point grid.

To validate whether it is legitimate to use QE results, we examine whether they correctly reproduce FP-LAPW calculations. Exchange and correlation effects were also treated within density-functional theory using the GGA + U in the SIC formalism [33] with $U = 5$ eV for the Fe-3*d* orbitals [17,36]. A $2 \times 2 \times 1$ k-point mesh was employed to sample the first Brillouin zone. The basis set size and muffin-tin radii were taken as in the case of the bulk system (Refs. [17] and [36]).

In both QE and FP-LAPW calculations atomic positions were optimized until obtain forces acting on all ion were smaller than 0.05 eV/Å. This tolerance value was taken because atomic displacements produced by forces smaller than 0.05 eV/Å results in changes in energies differences, magnetic moments or bond-lengths that are below our convergence error.

To check the precision of our calculations, we performed several additional calculations, following the procedure described by some of us in reference 17. By examining the effect of different basis sets and k-point grids (we considered $1 \times 1 \times 1$, $2 \times 2 \times 1$, $3 \times 3 \times 1$ and $4 \times 4 \times 2$ k-point grids) we conclude that for the parameters employed in the present ab initio study our results are very well converged, being these parameters an optimal compromise precision-computational times.

In contrast to a regular functional as PBE, the GGA + U method is not implemented in exactly the same way in the two employed codes. In the case of Wien2k the U correction is applied within the muffin tin spheres. A pseudopotential method as QE does not have this concept of muffin tin spheres. In consequence, differences between both methods are expected. We not pretend here to perform a deep comparison as

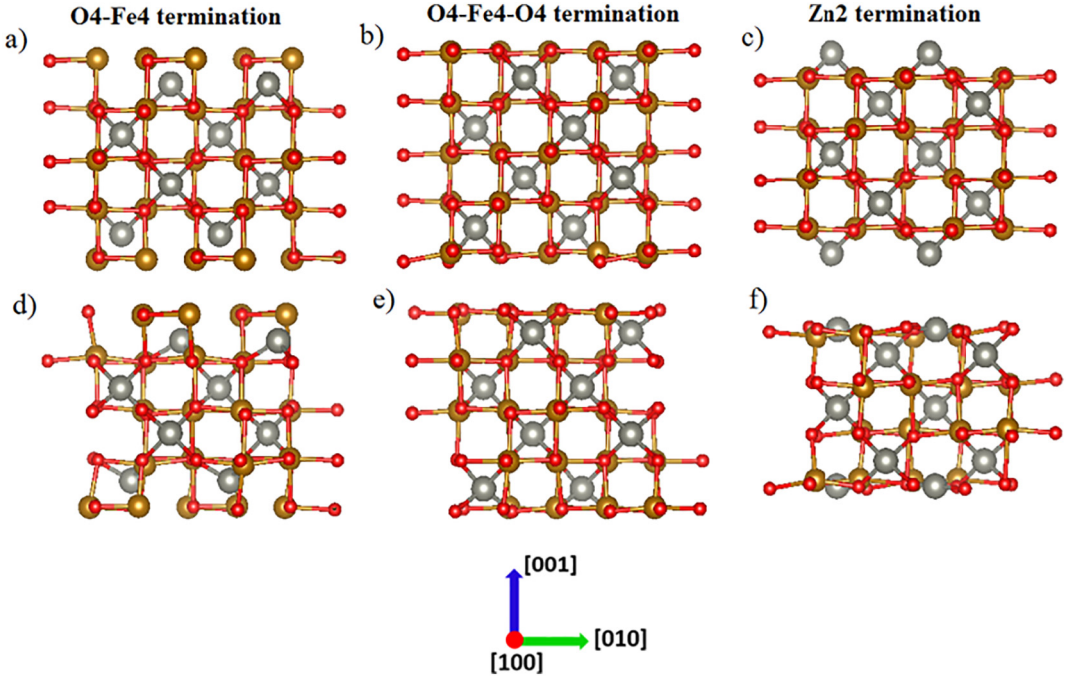

Fig. 1. Slab models for the different (001) surface terminations of $ZnFe_2O_4$. Top: Initial (un-reconstructed) structures of $ZnFe_2O_4$ (001) surface terminations. Bottom: Reconstructed structures.

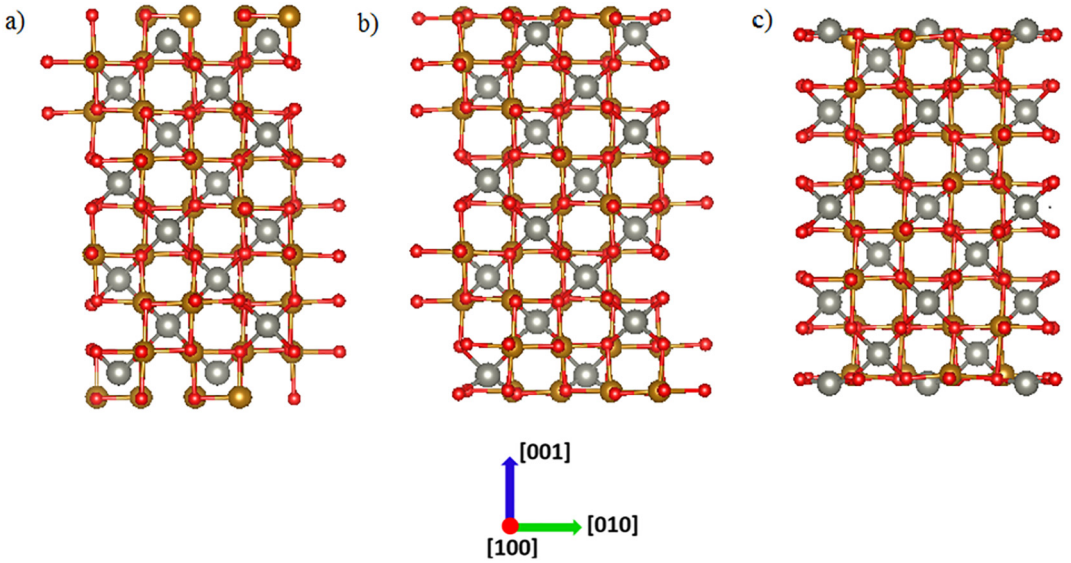

Fig. 2. 17 Å thickness slab model of $ZnFe_2O_4$ (001) surface terminations. a) O_4-Fe_4 termination. b) O_4-Fe_4-O_4 termination. c) Zn_2 termination. Only the reconstructed terminations are shown.

those presented in Ref. [37] for PBE calculations. We just want to have an estimation of the differences between both GGA + U methods.

We modeled the (001) surface terminations by using the slab-supercell approach. For the simulation of each termination we considered three different periodic slabs. Initially we study a slab composed by nine layers of Zn_2 and O_4-Fe_4-O_4 stacked alternately, separated by a vacuum space, see Fig. 1. Then, the unit cells used to simulate the fully terminated Zn_2, O_4-Fe_4 and O_4-Fe_4-O_4 (001) terminations contains 58, 60 and 68 atoms, respectively. The thickness of these slabs is 8.5 Å. Our calculations showed that 11 Å of vacuum is sufficient to decouple the slabs. FP-LAPW and QE calculations were performed for this 8.5 Å thickness slab. To ensure that artificial interaction between the upper and lower layers of the slab is negligible, QE calculations considering a 17.0 Å thickness slab were also performed. This slab is composed by 17 layers of Zn_2 and O_4-Fe_4-O_4 stacked alternately (Fig. 2). The slabs contain now 114, 116 and 124 atoms in the cases of the Zn_2, O_4-Fe and O_4-Fe_4-O_4 (001) surface terminations. These larger slabs were studied performing QE calculations only.

In Ref. [17] we reported that the lowest-energy configuration of normal $ZnFe_2O_4$ is antiferromagnetic with a = 8.46 Å and u = 0.260. This spin configuration is also the lowest energy one for the case of the different terminations studied here and then will be used as the starting ones for our study of the three (001) surface terminations previously described.

3. Results and discussion

We will start the discussion of the results obtained for the (001) surface terminations of $ZnFe_2O_4$ by the QE and FP-LAPW results obtained for the cases of the 8.5 Å thickness slab. QE and FP-LAPW predict the same results for the surface structure: in the cases of the Zn_2 and O_4-Fe_2-O_4 a strong surface reconstruction occurs. For the Zn_2 surface termination the superficial Zn atoms relax inward the sub-surface layer, being the magnitude of the Zn atoms displacement of about 1 Å (see Fig. 1d). In the case of the O_4-Fe_4-O_4 termination, the Zn atoms located in the sub-surface layer (1 Å below the O_4-Fe_4-O_4 superficial layer) relax outwards to the surface. The magnitude of the Zn atoms displacement along the z-direction is c.a. ~0.5 Å (see Fig. 1e). As a conclusion, we can point out that our ab initio calculations predict that, after the surface reconstruction, both terminations yield a similar structure with a O_4-Fe_4-Zn_2-O_4 superficial layer. In the case of the reduced O_4-Fe_4 surface termination, the surface reconstruction is less pronounced (see Fig. 1f). QE calculations predict very similar results for the structural properties of the (001) surface terminations of $ZnFe_2O_4$ when a slab of 17 Å thickness is considered.

It is important to mention that the structural reconstruction of the different (001) surface terminations of $ZnFe_2O_4$ implies a nearly vertical movement (z direction in Figs. 1 and 2) of the superficial and sub-superficial layers. More complex reconstructions (in which the two-dimensional symmetry of the surface in the x-y plane is altered) can be realized in a real sample. These reconstructions cannot be described with the slab used in the present work to simulate the surface terminations. In order to study these complex reconstructions the dimensions of the slab must be duplicated (at least) in the x and y directions. These slabs contain > 224 atoms plus the vacuum and requires extremely large computational times and resources.

In order to determine the stability of each surface termination we study the surface energy formation that was calculated as [38,39]:

$$\gamma = \frac{E_{slab} - [N_{Zn}\mu(Zn) + N_{Fe}\mu(Fe) + N_O\mu(O)]}{2A} \quad (1)$$

to take into account the different stoichiometries of each termination. In the above equation E_{slab} is the total energy of the slab structure considered N_{Zn}, N_{Fe}, and N_O are the number of Zn, Fe and O atoms in the slab (the number of Zn. Fe, and O atoms for each slab configuration is shown in Table 1). μ(Zn), μ(Fe) and μ(O) are the chemical potentials of Zn, Fe, and O that must satisfy:

$$E(ZFO) = \mu(Zn) + 2\mu(Fe) + 4\mu(O) \quad (2)$$

and

$$E(ZnO) = \mu(Zn) + \mu(O) \quad (3)$$

being E(ZFO) and E(ZnO) the total energies of one unit-formula of bulk

Table 1
Number of Zn, Fe, and O atoms (N_{Zn}, N_{Fe}, and N_O) in the slabs used for the simulation of the different (001) surface terminations of $ZnFe_2O_4$.

		N_{Zn}	N_{Fe}	N_O
8.5 Å thickness slab	Zn_2 termination	10	16	32
	O_4-Fe_4 termination	8	20	32
	O_4-Fe_4-O_4 termination	8	20	40
17 Å thickness slab	Zn_2 termination	18	32	64
	O_4-Fe_4 termination	16	36	64
	O_4-Fe_4-O_4 termination	16	36	72

$ZnFe_2O_4$ and ZnO, respectively.

The chemical potentials vary depending on the experimental environments in which the surface is growth, but there are upper and lower limits that define a range for the chemical potentials. The upper limit of μ(O) is the chemical potential of an oxygen molecule, $\mu(O_2)$. For μ(O) larger than $\mu(O_2)/2$ vaporization of oxygen as molecules from the $ZnFe_2O_4$ surfaces will occur. In the following we call this upper limit "O-rich environment". In this situation, $\mu(O^{rich}) = \mu(O_2)/2$. The lower limit of μ(O) correspond to the upper limits of μ(Zn) and μ(Fe) which is the Zn and Fe chemical potentials in metallic Zn and Fe. For larger values of μ(Zn) and μ(Fe) segregation of metallic Zn and Fe will occur. This is the "oxygen-poor environment".

In order to obtain the required chemical potentials FP-LAPW and QE calculations (with the same precision than those corresponding to the slab structures and bulk $ZnFe_2O_4$) for a O_2 molecule and metallic Zn, metallic Fe and ZnO were performed. It was found that $\mu(O^{poor})$-$\mu(O^{rich}) = -5.4$ eV for the present calculations. By using Eqs. (1)–(3) and the surface energy for the O-rich environment ($E^{O\ rich}$) we can write the surface energy as a linear function of the oxygen chemical potential:

$$\gamma = \frac{E^{O\ rich}}{2A} + \frac{\left[\frac{3}{2}N_{Fe} + N_{Zn} - N_O\right]}{2A}\Delta\mu \quad (4)$$

with $\Delta\mu = (\mu(O)\text{-}\mu(O^{rich}))$. From detailed convergence studies we determine that our precision error in γ is in the order of 10 meV/Å^2.

In a first stage we will analyse the stability of the normal (001) terminations. Fig. 3 shows the calculated surface energies γ as a function of the oxygen chemical potential for the case of the FP-LAPW calculations. The QE predictions for γ follow the same trend and predict that the Zn_2 surface termination has the lowest surface energy formation for the possible range of the oxygen chemical potential. In Table 2, the values of γ for the extreme oxygen potential range (O-rich and O-poor) are shown. We must pointed out here that the WIEN2k calculations predict negative values for γ in the case of the Zn_2 surface termination. This negative value, that do not appear for the case of the QE calculations, would indicate a qualitatively different prediction and this is not what one expects for two equivalent DFT methods. As can be seen in Table 2 the differences in the surface energy values between WIEN2k and QE roughly correspond to a rigid shift. The (unphysical) negative sign predicted by the Wien2k calculations is related to the model used for the calculation of the atomic energies used in Eqs. (1)–(3) systems for the calculation of γ (most probably the O_2-molecule), resulting in the rigid shift of the surface energies between both methods. For this reason, physical information is contained in the difference in the surface formation energies between terminations and not in its sign.

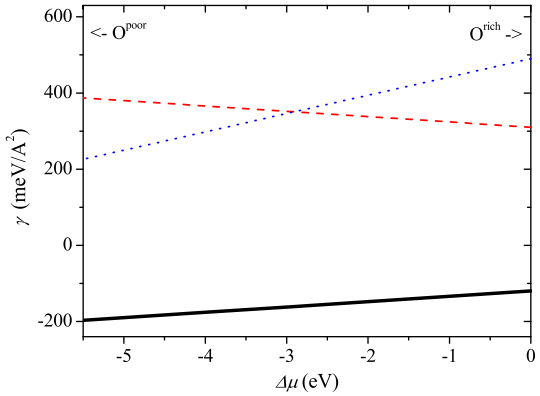

Fig. 3. Calculated surface energies (γ) for the three (001) terminations of $ZnFe_2O_4$ studied here. Dashed red, dotted blue, and solid black lines represent the surface energies of the terminations O_4-Fe_4-O_4, O_4-Fe_4 and Zn_2 terminations, respectively. The left and right *x*-axis ends correspond to the O-poor and O-rich environments. The calculations correspond to the FP-LAPW calculations, 8.5 Å thickness slab.

When the 17 Å thickness slabs are considered as a model for the simulation of the (001) terminations of $ZnFe_2O_4$ the QE calculations predict a similar trend, i.e., Zn_2 is the stable termination. Calculations performed using as a model for the surface a 25.5 Å thickness slab and 16 Å of vacuum confirm all the discussed results for the surface stability and confirms that even for the 8.5 Å slab thickness the spurious interaction between the upper and lower layers of the slab is negligible. As can be seen in Fig. 3, the O_4-Fe_4 termination is more stable than the O_4-Fe_4-O_4 in the O-poor environment. The inverse situation is observed, as expected, for the O-rich condition.

In Reference 40 it was shown that the surface energies obtained in PBE calculations overestimates the experimental values by about 12% and even after correcting for this bias there is a remaining ± 15 meV/Å^2 uncertainty on the resulting surface energy. From our convergence tests an estimate uncertainty of 10 meV/Å^2 in γ was derived. Even when the mentioned 12% overestimation correction, the convergence error and the remaining uncertainty are considered, the phase stability presented in Fig. 3 is not changed.

In Fig. 4 we present the QE results for the magnetic moments at the Fe sites for the case of the 17 Å thickness slab as a function of the distance of the Fe atom to the surface for the three terminations studied. As a general result we can see that Fe atoms in the surface present magnetic moments smaller than those located in the bulk. For the case of the O_4-Fe_4 and the O_4-Fe_4-O_4 terminations, the magnitude of the magnetic moment of the Fe atoms located in the superficial layer are 3.95 and 3.60 μ_B, respectively. This reduction of the magnetic moments of the Fe atoms located in the superficial layers of both terminations is associated to the change in the O-coordination of these Fe atoms and the subsequent changes in the charge in the atomic spheres of these Fe atoms (the reduction of the oxygen coordination of the Fe atoms at the surface induces an increment in the charge in this Fe atoms from 23.7*e* up to 23.9*e*). A similar effect was found in reduced bulk $ZnFe_2O_4$. In this case, the formation of an oxygen vacancy reduce the magnitude of the magnetic moments of the three Fe atoms nearest neighbors to the vacancy sites to from 4.2 μ_B [17] to 4.0 μ_B (two Fe atoms) and -3.6 μ_B for the remaining one [36]. The Fe atoms located in layers 2.3 Å (at least) below the surface present magnetic moments in the order of 4.1–4.2 μ_B. For both O_4-Fe_4 and O_4-Fe_4-O_4 terminations no spin-polarization was found at the Zn-sites while spin-polarization in the order of 0.15 μ_B was found for some oxygen atoms (a similar result was obtained in reduced $ZnFe_2O_4$, see Ref. [36]).

In the case of the Zn_2 surface termination, a different behavior was found. Similar to the previous cases, the Fe atoms located 1.3 Å below the surface present a spin-polarization of 4.0 μ_B, an expected reduction due to the smaller oxygen coordination of these Fe atoms compared to the case of bulk $ZnFe_2O_4$. But, the Fe atoms located 3.4 Å below the surface present even smaller magnetic moments, 3.6 μ_B. This result can be explained in terms of the superficial reconstruction and the charge rearrangement that induces: when the unreconstructed Zn_2 surface is inspected magnetic moments of ± 4.2 μ_B are predicted for Fe-atoms located at 3.4 Å from the surface. After the structural reconstruction (that implies a large displacement of the superficial Zn_2 atoms to the O_4-Fe_4-O_4 sub-surface layer) the magnetic moment of the Fe atoms of the sub-surface layers drops to ± 3.6 μ_B. For this Zn_2 termination, no magnetic moments were found at the Zn sites and some oxygen atoms present magnetic moments in the order of 0.10 μ_B. It is important to mention here that QE and FP-LAPW calculations performed in the 8.5 Å thickness slab predicts the same behavior for the magnetic moments (differences in the order of 0.2 μ_B between both methods).

After the study of the slabs with a normal distribution of Zn and Fe cations in the A and B sites of $ZnFe_2O_4$, we have considered the Zn-Fe anti-site defect formed by cation inversion between Zn and Fe atoms at superficial and deep layers. Our DFT-based calculations show that, independently of the surface termination considered, the normal structure and those with a superficial anti-site have the same energy (differences smaller than the convergence error), see Table 2. This result is

Table 2
Predicted surface energy formations γ (in meV/A^2) for the different terminations and slabs studied here by means of FP-LAPW and QE calculations.

		γ (meV/A^2) O_4-Fe_4-O_4 termination	γ (meV/A^2) O_4-Fe_4 termination	γ (meV/A^2) Zn_2 termination
O-rich condition				
FP-LAPW, 8.5 Å thickness slab	Normal	310	490	−120
	Superficial anti-site	310	490	−120
	Deep anti-site	310	500	−100
QE, 8.5 Å thickness slab	Normal	218	386	155
	Superficial anti-site	218	386	158
	Deep anti-site	216	395	202
QE, 17 Å thickness slab	Normal	222	390	158
	Superficial anti-site	223	390	161
	Deep anti-site	222	400	204
O-poor condition				
FP-LAPW, 8.5 Å thickness slab	Normal	380	260	−190
	Superficial anti-site	380	260	−190
	Deep anti-site	380	270	−170
QE, 8.5 Å thickness slab	Normal	293	159	80
	Superficial anti-site	293	159	83
	Deep anti-site	292	167	127
QE, 17 Å thickness slab	Normal	298	163	83
	Superficial anti-site	297	163	86
	Deep anti-site	298	172	128

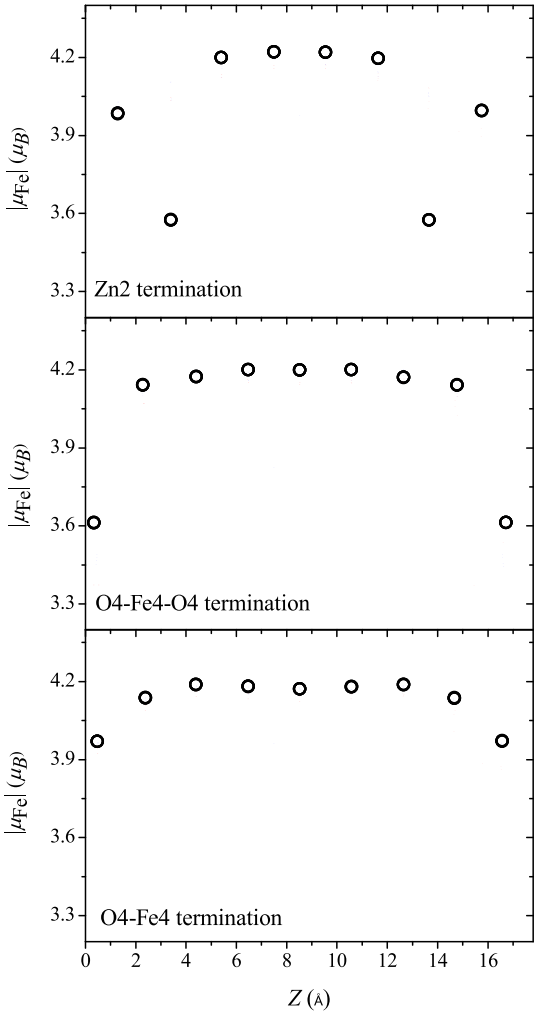

Fig. 4. Magnetic moment μ at the Fe sites as a function of the distance (in Å) to the surface (Z) for the three (001) surface terminations studied here. In all cases the results correspond to the normal structures. $Z = 0$ correspond to the lower layer of the slabs showed in Fig. 1. Magnetic moments at the Fe sites in bulk $ZnFe_2O_4$ are 4.2 μ_B.

contrary to those found in bulk $ZnFe_2O_4$, for which the inversion process is strongly endothermic: the normal structure has the lowest-energy, being the energy difference between the normal and partially inverted structure −85 meV per unit formula (*f.u.*) (Ref. [36]).

The superficial cation inversion is promoted by the rearrangement of the electronic structure in the surface layer in order to compensate the changes originated by the surface. As we discussed in a previous work, a similar effect is observed in volumetric and reduced $ZnFe_2O_4$: when an oxygen vacancy and one anti-site in the bulk structure is considered the energy necessary to produce a Zn-Fe anti-site is in the order of −30 meV/*f.u.*, 60% smaller than those required in the case of stoichiometric $ZnFe_2O_4$ [36]. These results show that the formation of oxygen vacancies or reduced coordination at the surfaces favours the cationic inversion in $ZnFe_2O_4$.

Based in our results we can conclude that Zn-Fe inversion is not a trapped defect (as in the bulk case) but also an integral component of the surface of $ZnFe_2O_4$. This conclusion is in agreement with experimental results that shown that the degree of cation inversion may scale with the surface area in $MgAl_2O_4$, $ZnFe_2O_4$, and $NiFe_2O_4$ ferrites spinel powders [21] or thin films [41]. In other works, it was shown that $ZnFe_2O_4$ nanoparticles of 6 nm diameter present a high degree of inversion that is associated to surface effects, i.e., involves cations allocated at the surface layer [42,43]. A similar result was obtained by Rasmussen et al. [38] in $MgAlO_4$ spinel, suggesting that surface-induced inversion could a general phenomenon in spinel-type oxides.

Concerning magnetic moments at the Fe sites, the same results previously discussed for normal $ZnFe_2O_4$ were found. The only difference is that the magnetic moments of the Fe atoms now allocated at the A-sites are 0.1–0.2 μ_B smaller than those of the Fe atoms that remain at the B-sites. This diminution is observed for Fe atoms allocated at the A sites in the surface layer or even in deep layers. For the case of the 17 Å slab, the Fe atoms located at A sites in deep layers (8.5 Å from the surfaces) present magnetic moments close to 4.2 μ_B, the same value predicted for Fe at the B-sites.

There is a last point to discuss: the ferrimagnetic response experimentally observed in nano-size zinc ferrite [20,43]. In this case we take the Zn_2 terminated reconstructed slab with one superficial anti-site and we study different ferromagnetic spin configurations in addition to the antiferromagnetic ones. We found that the lowest-energy magnetic configuration corresponds to a ferrimagnetic system with a net magnetic moment of 1.2 μ_B/Fe atom. For the case of the normal slab the lowest-energy solution is the antiferromagnetic one. This result shows

that the surface (reduced Fe-coordination) favours the cationic inversion and in turns the cationic inversion favours ferrimagnetic configurations. A systematic study of the magnetic behavior of the surface terminations of $ZnFe_2O_4$ is now in progress.

4. Conclusions

In this work we have study, by using two different DFT-based methods (all electron FP-LAPW and plane wave and pseudopotentials method as implemented in the Quantum Espresso code) the stability of the Zn_2, O_4-Fe_4 and O_4-Fe_4-O_4 terminations of the (001) surface of $ZnFe_2O_4$, considering slabs of 8.5 Å and 17 Å thickness. We found that, after the surface reconstruction, the Zn2 termination is the stable one. We also found that cationic inversion, a defect in volumetric $ZnFe_2O_4$, become energetically favourable in the surface. This result explains the high degree of inversion observed in nano-sized and thin films of $ZnFe_2O_4$. The presence of some inversion degree in the samples gives rise to Fe^A–O–Fe^B couplings that strengthen the magnetic interactions and the ferrimagnetic behavior at high temperatures. Calculations of the magnetic coupling constants in normal and inverted bulk and thin films of $ZnFe_2O_4$ are now in progress in order to correlate the degree of inversion with the magnetic behavior of this semiconducting oxide.

Acknowledgments

This research was partially supported by CONICET (Grant No. PIP0747, PIP0720), UNLP (Grant No. 11/X678, 11/X680, 11/X708, 11/X788, 11/X792), ANPCyT (Grant No. PICT PICT 2012-1724, 2013-2616, 2016-4083) and UNNOBA (Grant No. SIB 0176-2017), and "Proyecto Acelerado de Cálculo 2017", Red Nacional de Computación de Alto Desempeño (SNCAD-MINCyT) - HPC Cluster, Rosario, Argentina. Funded by the Deutsche Forschungsgemeinschaft (DFG, German Research Foundation)–Projektnummer 31047525-SFB 762, Projects A4 and B1.

References

[1] J. Smit, H.P.J. Wijn, Ferrites, Philips Technical Library, Eindhoven, 1959.
[2] Chao Jin, Peng Li, Wenbo Mi, Haili Bai, Structure, magnetic, and transport properties of epitaxial $ZnFe_2O_4$ films: an experimental and first-principles study, J. Appl. Phys. 115 (2014) 213908.
[3] Y. Kajiwara, K. Harii, S. Takahashi, J. Ohe, K. Uchida, M. Mizuguchi, H. Umezawa, H. Kawai, K. Ando, K. Takanashi, S. Maekawa, E. Saitoh, Transmission of electrical signals by spin-wave interconversion in a magnetic insulator, Nature 464 (2010) 262–266.
[4] C.E. Rodríguez Torres, F. Golmar, M. Ziese, P. Esquinazi, S.P. Heluani, Evidence of defect-induced ferromagnetism in $ZnFe_2O_4$ thin films, Phys. Rev. B 84 (2011) 064404.
[5] K. Kamazawa, Y. Tsunoda, H. Kadowaki, K. Kohn, Magnetic neutron scattering measurements on a single crystal of frustrated $ZnFe_2O_4$, Phys. Rev. B 68 (2003) (024412 and references there in).
[6] Y. Yamada, K. Kamazawa, Y. Tsunoda, Interspin interactions in $ZnFe_2O_4$: theoretical analysis of neutron scattering study, Phys. Rev. B 66 (2002) 064401.
[7] K. Kamazawa, Y. Tsunoda, K. Odaka, K. Kohn, Spin liquid state in $ZnFe_2O_4$, J. Phys. Chem. Solids 60 (1999) 1261–1264.
[8] W. Schiessl, W. Potzel, H. Karzel, M. Steiner, G.M. Kalvius, A. Martin, M.K. Krause, I. Halevy, J. Gal, W. Schäfer, G. Will, M. Hillberg, R. Wäppling, Magnetic properties of the $ZnFe_2O_4$ spinel, Phys. Rev. B 53 (1996) 9143–9152.
[9] T. Usa, K. Kamazawa, H. Sekiya, S. Nakamura, Y. Tsunoda, K. Kohn, M. Tanaka, Magnetic properties of $ZnFe_2O_4$ as a 3-D geometrical spin frustration system, J. Phys. Soc. Jpn. 73 (2004) 2834–2840.
[10] K. Tomiyazu, K. Kamazawa, A spin molecule model for geometrically frustrated spinel $ZnFe_2O_4$, J. Phys. Soc. Jpn. 80 (2011) SB024.
[11] M.A. Hakim, M. Manjurul Haque, M. Huq, P. Nordblad, Spin-glass-like ordering in the spinel $ZnFe_2O_4$ ferrite, Physica B 406 (2001) 48–51.
[12] J.L.G. Fierro, Metal Oxides—Chemistry and Applications, Taylor and Francis, Boca Raton, Fl, 2006.
[13] R.E. Vandenberghe, E. De Grave, Mösbauer Spectroscopy Applied to Inorganic Chemistry, vol. 3, Plenum, New York, 1989.
[14] M. Niyaifar, Effect of preparation on structure and magnetic properties of $ZnFe_2O_4$, J. Magn. 19 (2014) 101–105.
[15] S.D. Jackson, Metal Oxide Catalysis, vol. 2, Wiley-VCH Verlag GmbH & Co, Weinheim, 2009.
[16] G.A. Pettit, D.W. Forester, Mössbauer study of cobalt-zinc ferrites, Phys. Rev. B 4 (1971) 3912–3923.
[17] J.J. Melo Quintero, C.E. Rodríguez Torres, L.A. Errico, Ab initio calculation of structural, electronic and magnetic properties and hyperfine parameters at the Fe sites of pristine $ZnFe_2O_4$, J. Alloy Compd. 741 (2018) 746–755.
[18] C.E. Rodríguez Torres, G.A. Pasquevich, P. Mendoza Zélis, F. Golmar, S.P. Heluani, Sanjeev K. Nayak, Waheed A. Adeagbo, Wolfram Hergert, Martin Hoffmann, Arthur Ernst, P. Esquinazi, S.J. Stewart, Oxygen-vacancy-induced local ferromagnetism as a driving mechanism in enhancing the magnetic response of ferrites, Phys. Rev. B 89 (2014) 104411.
[19] M. Mozaffari, M. Eghbali Arani, J. Amighian, The effect of cation distribution on magnetization of $ZnFe_2O_4$ nanoparticles, J. Magn. Magn. Mater. 322 (2010) 3240–3244.
[20] B. Pandey, F.J. Litterst, E.M. Baggio-Saitovitch, Preferential spin canting in nanosize zinc ferrite, J. Magn. Magn. Mater. 385 (2015) 412–417.
[21] V. Sepelák, S. Indris, P. Heitjans, K.D. Becker, Direct determination of the cation disorder in nanoscale spinels by NMR, XPS, and Mossbauer spectroscopy, J. Alloy Compd. 434–435 (2007) 776–778.
[22] U. Köning, E.F. Bertaut, Y. Gros, G. Chol, Models of the magnetic structure of zinc ferrite, Solid State Commun. 8 (1970) 759–764.
[23] B.J. Evans, S.S. Hafner, H.P. Weber, Electric field gradients at ^{57}Fe in $ZnFe_2O_4$ and $CdFe_2O_4$, J. Chem. Phys. 55 (1971) 5282–5288.
[24] A. Kremenovica, B. Antic, P. Vulic, J. Blanusa, A. Tomic, $ZnFe_2O_4$ antiferromagnetic structure redetermination, J. Magn. Magn. Mater. 426 (2017) 264–266.
[25] J.A. Gomes, M.H. Sousa, F.A. Tourinho, J. Mestnik-Filho, R. Itri, J. Depeyrot, Rietveld structure refinement of the cation distribution in ferrite fine particles studied by X-ray powder diffraction, J. Magn. Magn. Mater. 289 (2005) 184–187.
[26] E. Sjöstedt, L. Nordström, D.J. Singh, An alternative way of linearizing the augmented plane-wave method, Solid State Commun. 114 (2000) 15–20.
[27] G.K.H. Madsen, P. Blaha, K. Schwarz, E. Sjöstedt, L. Nordström, Efficient linearization of the augmented plane-wave method, Phys. Rev. B 64 (2001) 195134.
[28] S. Cottenier, Density Functional Theory and the Family of (L)APW-methods: a Step-by-Step Introduction, KU Leuven, Belgium, 2002. http://www.wien2k.at/reg_user/textbooks. 2013 (accessed July 2019).
[29] P. Blaha, K. Schwarz, G. Madsen, D. Kvasnicka, J. Luitz, WIEN2k, an Augmented Plane Wave Plus Local Orbitals Program for Calculating Crystal Properties, Technical Universität Wien, Austria, 1999.
[30] P. Giannozzi, O. Andreussi, T. Brumme, O. Bunau, M. Buongiorno Nardelli, M. Calandra, R. Car, C. Cavazzoni, D. Ceresoli, M. Cococcioni, N. Colonna, I. Carnimeo, A. Dal Corso, S. de Gironcoli, P. Delugas, R.A. DiStasio Jr., A. Ferretti, A. Floris, G. Fratesi, G. Fugallo, R. Gebauer, U. Gerstmann, F. Giustino, T. Gorni, J. Jia, M. Kawamura, H.-Y. Ko, A. Kokalj, E. Küçükbenli, M. Lazzeri, M. Marsili, N. Marzari, F. Mauri, N.L. Nguyen, H.-V. Nguyen, A. Otero-de-la-Roza, L. Paulatto, S. Poncé, D. Rocca, R. Sabatini, B. Santra, M. Schlipf, A.P. Seitsonen, A. Smogunov, I. Timrov, T. Thonhauser, P. Umari, N. Vast, X. Wu, S. Baroni, Advanced Capabilities for Materials Modelling With QUANTUM ESPRESSO, vol. 29, (2017), p. 465901.
[31] P. Giannozzi, et al., QUANTUM ESPRESSO: a modular and open-source software project for quantum simulations of materials, J. Phys.-Condens. Mat. 21 (2009) (2009) 395502.
[32] J.P. Perdew, A. Ruzsinszky, G.I. Csonka, O.A. Vydrov, G.E. Scuseria, L.A. Constantin, X. Zhou, K. Burke, Restoring the density-gradient expansion for exchange in solids and surfaces, Phys. Rev. Lett. 100 (2008) 136406.
[33] V.I. Anisimov, I.V. Solovyev, M.A. Korotin, M.T. Czyzyk, G.A. Sawatzky, Density functional theory and NiO potoemission spectra, Phys. Rev. B 48 (1993) 16929–16934.
[34] G. Prandini, A. Marrazzo, I.E. Castelli, N. Mounet, N. Marzari, Precision and efficiency in solid-state pseudopotential calculations, npj Comput. Mater. 4 (2018) 72.
[35] H.J. Monkhorst, J.D. Pack, Special points for Brillouin-zone integrations, Phys. Rev. B 13 (1976) 5188–5192.
[36] J.J. Melo Quintero, K.L. Salcedo Rodríguez, C.E. Rodríguez Torres, L.A. Errico, Ab initio study of the role of defects on the magnetic response and the structural, electronic and hyperfine properties of $ZnFe_2O_4$, J. Alloy Compd. 775 (2019) 1117–1128.
[37] K. Lejaeghere, G. Bihlmayer, T. Björkman, P. Blaha, S. Blügel, V. Blum, D. Caliste, I.E. Castelli, S.J. Clark, A. Dal Corso, S. de Gironcoli, T. Deutsch, J.K. Dewhurst, I. Di Marco, C. Draxl, M. Dułak, O. Eriksson, J.A. Flores-Livas, K.F. Garrity, L. Genovese, P. Giannozzi, M. Giantomassi, S. Goedecker, X. Gonze, O. Grånäs, E.K.U. Gross, A. Gulans, F. Gygi, D.R. Hamann, P.J. Hasnip, N.A.W. Holzwarth, D. Iuşan, D.B. Jochym, F. Jollet, D. Jones, G. Kresse, K. Koepernik, E. Küçükbenli, Y.O. Kvashnin, I.L.M. Locht, S. Lubeck, M. Marsman, N. Marzari, U. Nitzsche, L. Nordström, T. Ozaki, L. Paulatto, C.J. Pickard, W. Poelmans, M.I.J. Probert, K. Refson, M. Richter, G. Rignanese, S. Saha, M. Scheffler, M. Schlipf, K. Schwarz, S. Sharma, F. Tavazza, P. Thunström, A. Tkatchenko, M. Torrent, D. Vanderbilt, M.J. van Setten, V. Van Speybroeck, J.M. Wills, J.R. Yates, Guo-Xu Zhang, S. Cottenier, Reproducibility in density functional theory calculations of solids, Science 351 (2016) 1415.
[38] M.K. Rasmussen, A.S. Foster, B. Hinnemann, F.F. Canova, S. Helveg, K. Meinander, N.M. Martin, J. Knudsen, A. Vlad, E. Lundgren, A. Stierle, F. Besenbacher, J.V. Lauritsen, Stable cation inversion at the $MgAl_2O_4$ (100) surface, Phys. Rev. Lett. 107 (2011) 036102.
[39] T. Kurita, K. Uchida, A. Oshiyama, Atomic and electronic structures of α-Al_2O_3 surfaces, Phys. Rev. B 82 (2010) 155319.
[40] S. De Waele, K. Lejaeghere, M. Sluydts, S. Cottenier, Error estimates for density-functional theory predictions of surface energy and work function, Phys. Rev. B 94 (2016) 235418.
[41] K.L. Salcedo Rodriguez, M. Hoffmann, F. Golmard, G. Pasquevicha, P. Werner,

W. Hergert, C.E. Rodriguez Torres, Producing $ZnFe_2O_4$ thin films from ZnO/FeO multilayers, Appl. Surf. Sci. 393 (2017) 256–261.

[42] J.M. Ramallo López, S.G. Marchetti, J.F. Bengoa, R.J. Prado, F.G. Requejo, S.J. Stewart, S.J.A. Figueroa, Cationic exchange in nanosized $ZnFe_2O_4$ spinel revealed by experimental and simulated near-edge absorption structure, Phys. Rev. B 75 (2007) 073408.

[43] S.J. Stewart, S.J.A. Figueroa, M.B. Sturla, R.B. Scorzelli, F. García, F.G. Requejo, Magnetic $ZnFe_2O_4$ nanoferrites studied by X-ray magnetic circular dichroism and Mössbauer spectroscopy, Physica B 389 (2007) 155–158.